ELSEVIER

Contents lists available at ScienceDirect

Composites Part B

journal homepage: www.elsevier.com/locate/compositesb





Water purification performance and energy consumption of gradient nanocomposite membranes

Yuchen Liu^a, Zimeng Zhang^a, Wei Li^a, Ruochen Liu^b, Jingjing Qiu^c, Shiren Wang^{a,b,*}

- ^a Department of Industrial and Systems Engineering, Texas A&M University, College Station, TX, 77843, USA
- b Department of Materials Science and Engineering, Texas A&M University, College Station, TX, 77843, USA
- ^c Department of Mechanical Engineering, Texas Tech University, Lubbock, TX, 77409, USA

ARTICLE INFO

Keywords: Gradient structure Graphene oxide Nanocomposite membrane Desalination Energy saving

ABSTRACT

Reverse Osmosis (RO) membrane-based desalination technology accounts for 2/3 water desalination installation capacity all over the world but suffers from intensive energy consumption, where the membrane filtration process accounts for \sim 71% of total energy consumption. In this research, gradient membranes were designed and assembled with graphene oxide and celluloses laminates, and then used for RO desalination. The water flowing path was tuned by graphene oxide sizes while salt/water separation was tailored by the graphene oxide interlayer crosslinking. The resultant gradient nanocomposite membranes demonstrated a water yield as high as $21.34 \text{ L h}^{-1} \text{ m}^{-2} \text{ bar}^{-1}$ with a salt rejection rate of 96.08% when the graphene oxide lateral size was reduced to 300 nm, and such a yield was 5 times higher than that of current commercial RO membranes. In addition, such a gradient nanocomposite membrane also resulted in a 35.8% energy-saving in the membrane filtration process. Furthermore, the gradient nanoporous structure also exhibits decent scalability and long-time stability.

1. Introduction

Reverse Osmosis (RO) desalination is a water purification process that uses semi-permeable thin membranes to pass pure water while rejecting the salts and other impurities [1]. Compared with thermal distillation and other desalination methods (including ion-exchange membrane processes, freezing desalination, geothermal desalination, eletrodeionisation (EDI) and solar desalination), RO desalination shows great advantages on the continuous process, mild working condition, low environmental pollution, and easy operation [2,3]. As a matter of fact, over 65% of current installed desalination capacity is based on the RO membrane process [4]. However, one of the most significant barriers for extending RO desalination technology to broader applications is the intensive energy consumption of the RO unit, which represents 50%-60% of the total cost of the whole desalination process [5]. In a typical seawater desalination plant that purifies Pacific Ocean water with total dissolved solids (TDS) of 33.5 g/L (33,500 ppm), the overall energy consumption is 3.57 kWh/m [3], and the RO unit accounts for 71% of this total energy consumption [6]. Besides the seawater, brackish water is another source for portable water recovery. U.S. Geological Survey indicated that brackish groundwater could help stretch limited freshwater supplies [7]. For brackish water RO desalination, the requirement on salt rejection rate is not as strict as that for seawater due to a lower ion concentration. The rejection rate of ~90% is pretty decent in converting brackish water into freshwater. Generally, the specific energy consumption (SEC) during the RO desalination process can be broke down into filtration resistance energy-consumption (SEC_f), which is related to the performance of the RO membrane, and other energy consumptions that are influenced by the system process and the feed water osmotic pressure [8]. Under the same RO desalination operating systems and feed salinity, the energy consumed by SECf is the main part that can be reduced, and this is one of the most significant criteria to evaluate the performance of a RO membrane. The energy consumption in the membrane filtration process can be ascribed to the steric effect and friction losses. Herein, reducing the steric effect and friction losses of water molecules from hydrodynamic theory is a very promising strategy. Although the mechanism of water molecule transportation through nanochannels is not clear [9], the water permeance was found to be negatively related to the length of water-transport pathway and the salt rejection rate depends on the stability of nanochannels [10].

Currently, commercial RO membranes are mainly made of polyamide (PA) thin composite film (TCF) and its derivatives, which suffer low water permeability, high energy consumption, high fouling tendency, and limited lifetime [11]. Even though some efforts have been

^{*} Corresponding author. Department of Industrial and Systems Engineering, Texas A&M University, College Station, TX, 77843, USA. E-mail address: s.wang@tamu.edu (S. Wang).

made, current RO membranes used in desalination are still suffering intensive energy consumption and low energy-efficiency. Emerging selectively-permeable membranes with sub-nanometer channels attract considerable attention for energy-efficient desalination [12–14]. A lot of nanomaterials, such as zeolites, metal-organic frameworks (MOF), ceramics, graphene, carbon nanotubes, and aquaporin (AQP), have been attempted to fabricate RO membranes [15–21]. Among all kinds of nanomaterials, graphene oxide (GO) has emerged as the most attractive one for water desalination because of outstanding antifouling and barrier performance in molecular separation due to its unique molecular structure, high tensile strength, and impermeability to small molecules.

Single-layer GO with ~1 nm pores has been studied for RO desalination [22,23]. However, it is extremely challenging to perforate 1 nm nanopores in a single-layer defect-free graphene nanosheet in a scalable way although large pores are readily percolated by numerous methods [24,25]. Yang et al. [24] fabricated large-area graphene nanomesh (GNM) through oxygen plasma with the mask made of single-walled carbon nanotubes (SWNT). GNM/SWNT nanocomposite exhibited extremely high water permeance of 24 L/(m² h bar), which was 30 times larger than that of single-layer graphene with SWNT and retained a salt rejection of up to 95.3% after 24 h of osmotic operation. However, the cost of large-scale single-layer graphene and the uneven size of the nanopores may be the barrier for broadening this technique into industrial applications. Vertically aligned GO-based membranes have also been attempted for RO desalination. Abraham et al. tuned the interlayer spacing of GO membrane to reach the 1 nm level by varying the humidity of the environment [25]. They ingeniously used the cross-sectional area for water desalination where the membrane was encapsulated by epoxy and the water flux reached 5 L m⁻² h⁻¹. However, it is also challenging to scale up. Another strategy was to use laminated GO nanosheets and tune the interlayer spacing through different kinds of intercalating materials to tailor nanochannels between GO layers. Many different spacers have been attempted to tune the GO interspacing after a group of researchers from Manchester University first studied the stacked graphene oxides layers for water desalination in 2014 [26]. The most popular spacers include carbon dots [27], SWNT [28], cations [29], small molecule monomers [30], and C60³¹. Although laminated GO nanosheets are scalable, different spacers significantly affect the scale-up capability, performance, and energy consumption of water desalination [32,33].

In this paper, a nanocomposite membrane consisting of ultrathin GO laminates with 1-nm channels and two porous cellulose layers is presented to achieve both energy efficiency and scalability for RO desalination. The GO laminates thickness and GO nanosheet lateral size were studied to reduce energy consumption while maintaining the water desalination performance. The stability and lifetime of the gradient GO membrane were also discussed at such low energy consumption. Finally, the scalability of the gradient structure is also presented to examine the potential of commercialization.

2. Experimental

2.1. Materials

Graphite flakes were provided by Asbury Carbons, US. Mixed cellulose esters (MCE) membranes were purchased from Millipore Inc. *p*-Phenylenediamine (PPD) (98%, HPLC), fuming nitric acid (>90%), sodium chlorate (>99.0%), sodium hydroxide (>98.0%), ammonia solution (25%) and butyl alcohol (>99.5%) were purchased from Sigma Aldrich. Methanol was purchased from VWR International LLC. All the chemicals were used as received.

2.2. Design and simulation

The 'Transport of Diluted Species in Porous Media', 'Thin-Film Flow, Domain', and 'Fluid-Solid Interaction' physics models in COMSOL were

applied to simulate the ion/water separation process and stress distribution in the membrane. The simulation cell for the aperture selection of the protective layer was rectangular with a fixed thickness of 10 nm and a varied width ranging from 25 nm to 200 nm. The fluid domain was also rectangular with a height of 30 nm and the same width as the membrane. The input pressure, density, and dynamic viscosity of seawater were set to 1 MPa, $1.03\times10^3~{\rm kg/m}$ [3], and 8.9×10^{-4} Pa s respectively. The Young's moduli of thin membranes were measured by DMA 850(TA Instruments) in the tensile mode. The simulation cell for the protective layer was rectangular with a height of 20 nm and a width of 200 nm. The porosity domain as the protective layer on the GO membrane was also rectangular with a 200 nm width and different thicknesses. The porosity of the protective layer was set to 70% according to the commercial data. Other parameters were described in the Supplementary Materials.

2.3. Preparation of gradient nanocomposite membrane

GO powders were prepared from graphite powder following modified Brodie's method according to our previous work [31]. The detailed synthesis route is stated in Supplementary Materials, 5 mg of as-prepared dry GO powder was dispersed into 100 mL DI water, and a droplet of ammonia solution was added to the GO dispersion to tune the pH value to 10-11. After 30min bath sonication, GO dispersion was centrifuged at 4400 rpm for 20 min to remove large particles. The amplitude and power density of the tip sonicator were set to 25% and 12.5 W/mL, respectively. Subsequently, the GO dispersion was treated by tip sonication for 0 min, 3 min, 10 min, and 20 min, resulting in GO nanosheets with a lateral size of 1430 nm, 1009 nm, 473 nm, and 276 nm, respectively. 0.01 M PPD was then added to the resultant GO dispersion under stirring. The resultant GO-PPD dispersion(e.g., 2 mL, 4 mL, 6 mL, or 8 mL) was pumped through an MCE filter membrane (25 nm aperture size with 47 mm in diameter) to produce GO/MCE membranes, where GO film thickness was dependent on the GO-PPD dispersion volume. The resultant 2-layered GO-MCE membrane was then covered by another MCE filter membrane and pressed by a Heat Presses (Digital Knight, K20 SP) at 80 °C with 20 psi pressure for 1 h.

2.4. Characterization

Zeta potential of GO dispersion was characterized by Dynamic Light Scattering (Zetasizer Nano ZS). GO nanosheet lateral size was measured by Dynamic Light Scattering (Zetasizer Nano ZS) and atomic force microscope (AFM, Bruker MultiMode 8) in tapping mode. The tensile strengths of GO films were tested by Dynamic Mechanical Analyzer (TA Instruments, Q850 with accessories). The GO sample for the AFM characterization was prepared by the following steps. Firstly, the GO dispersion was diluted with 10-times DI water. Then a droplet of diluted GO dispersion was dropped on a clean silicon wafer followed by blowing dry with nitrogen. X-ray diffraction (XRD) characterization of the MCE/ GO membrane was carried out by Bruker D8 ECO diffractometer with a copper target (Kα1 radiation wavelength 1.54056 Å). ATR-FTIR characterization was carried out by the ATR-FTIR spectrometer (Bruker Alpha-Platinum). The MCE/GO/MCE gradient membrane was dipped into a plastic tube of epoxy resins for 24 h, and then the samples were encapsulated by the cured epoxy resin. The plastic tube was then cut by waterjet cutter, and the cross-section was characterized by scanning electron microscopy (SEM, JEOL JSM-7500F).

2.5. Desalination test

The water desalination tests were carried out by an in-house built system (Inset images of Fig. 4(b)). Specifically, 40 mL saline water with 2000 ppm NaCl was added into the feed side. The applied pressure on the feed side was 2.68 bar. The permeant water was collected by a measuring cylinder which is sealed by a tin foil to avoid potential

evaporation of water. Electrical conductivity was measured by a conductivity meter (Horiba B-771 Twin Conductivity/Salinity Tester).

Total Dissolved Solids (TDS) and electrical conductivity (EC) of the saline water can be calculated using the following equation:

$$TDS(mg/L) = k \cdot EC(\mu S/cm) \tag{1}$$

where k is the TDS factor for the solutions.

For NaCl solution, $k=0.48\pm0.01$ when the EC is in the range of 100–2000 uS/cm at the temperature of 25°C. Since the solute in the solution is NaCl only, the TDS can be converted to the ion concentration of NaCl solution by the following equation:

$$TDS(mg/L) = C(mol/L) \cdot M(mg/mol)$$
(2)

$$C(mol/L) = \frac{k \cdot EC(\mu S/cm)}{M(me/mol)}$$
(3)

where C is the ion concentration of the solution, M is the mole mass of the solute, which is 58,440 mg/mol for NaCl.

The salt rejection rate was calculated by the following equation:

$$R = \left(1 - \frac{C_p}{C_f}\right) \times 100\% \tag{4}$$

where Cp and Cf are the ion concentrations in permeate and feed side of solutions respectively.

2.6. Scale-up demonstration

The large-size membrane was fabricated by a homemade setup (Fig. S7 in the supplementary). As-prepared scale-up GO/MCE membrane was also bonded by another MCE membrane to form the gradient structure with the same steps as mentioned above. The resultant large-size membrane was cut to 47 mm disks for desalination tests.

3. Results and discussion

A nanocomposite membrane consisting of an ultrathin GO film and two MCE films is illustrated in Fig. 1. The 1-nm channels in the GO membrane were tuned by the GO interlayer bonding and two porous layers with a pore size of $2–50~\rm nm$ serving as the support and protective layer for RO desalination.

The gradient nanocomposite shows both gradient aperture size and gradient thickness. The mesoporous layer was made of MCE and was used to protect the ultrathin GO laminates from damage caused by large hydrodynamic pressure due to water flow. The middle GO laminates serve as the essential ion sieving layer through 1 nm-channel of inter-GO spacing, and the primary energy consumption occurs at this layer. 1 nm channels in the middle layer ensure high salt-rejection while the ultrathin thickness of the 1 nm-channel layer ensures high water-flux and low energy consumption. The thickness of GO laminates and the lateral size of GO nanosheets were tailored to reduce the energy consumption while

water desalination performance was maintained. The stability and lifetime of the gradient GO membrane were also discussed at such a low energy consumption. Finally, the scalability of the gradient structure was also presented to examine the potential of commercialization.

High water permeability requires large pores while high selectivity requires ultra-small pores, typically ~1 nm pore size. The gradient structure can perfectly solve this conflict by implementing ion sieving in the middle layer, which primarily contributes to energy consumption. Minimizing the ion sieving paths can minimize ion sieving energy consumption and also increase water permeability. A straightforward strategy is to minimize the thickness of the GO laminates since vertically-aligned GO nanosheets are difficult to be scaled-up. Meanwhile, minimizing the GO laminate thickness could significantly weaken its mechanical strength, resulting in poor robustness and a very short lifetime. Therefore, the conflicts between low energy consumption and a long lifetime should be solved. During the RO desalination, the tensile stress applied to the RO membrane comes from the friction between the fluid and solid membrane, and the hydraulic pressure difference between the feed-side flow and permeate-side flow. To maintain the longterm stability of desalination performance, the membrane should be robust enough to avoid any rupture. To ensure outstanding performance of ultrathin GO laminate, one of the most feasible strategies is to add a protective layer. Since it is difficult to directly measure the stress experienced by the membrane during the desalination process, a numerical simulation was performed by COMSOL Multiphysics to investigate the role of the protective layer on the stress reduction and to guide the design. The detailed model generation procedure was provided in the Method Section and Supplementary Materials.

Generally, increasing the thickness of the protective layer can reduce the tensile stress applied to the GO laminates. To understand the effect of MCE layer thickness on the GO laminate robustness, a physical model was built for a fixed pore size. Considering a typical operating pressure was above 10 bar (1 MPa), the feed flow of 1 MPa was assumed for the simulation. For the MCE membranes with 25 nm pores and 72% porosity (based on experimental characterization of such an MCE membrane), the resultant hydrodynamic stress loaded on 30 nm-thick GO laminates was simulated as shown in Fig. 2 (a). In this figure, the pressure distribution of the cross-sectional view of the membrane was shown by different color labels for different MCE thicknesses. The maximum tensile stress loaded on the 30-nm-thick GO laminates without the protective layer was found to be 2250 MPa which could significantly damage the GO laminates. As the thickness of the MCE layer increased from h = 0 nm to h = 1000 nm, the maximum tensile stress decreased exponentially to 3.92 MPa, a much smaller value than the threshold where the GO laminates can be damaged. Therefore, the thickness of the MCE layer would significantly influence the hydrodynamic stress loaded on the GO laminates. This could be ascribed to the protective layer that can bind the boundary of the GO laminates to reduce deformation area. The smaller deformation of GO laminates indicates smaller tensile stress. According to the tensile test of ultrathin GO laminates which is shown in Fig. S3, the resultant GO laminates showed a tensile strength of \sim 120

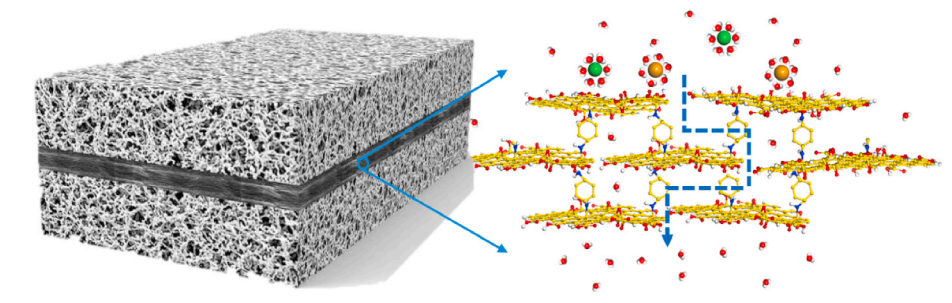


Fig. 1. Schematic illustration of nanocomposite membrane consisting of GO laminates with 1 nm channels and two symmetric mesoporous (2–50 nm pore size) layers. The ion is sieved via the middle layer, 1 nm-channels GO laminates.

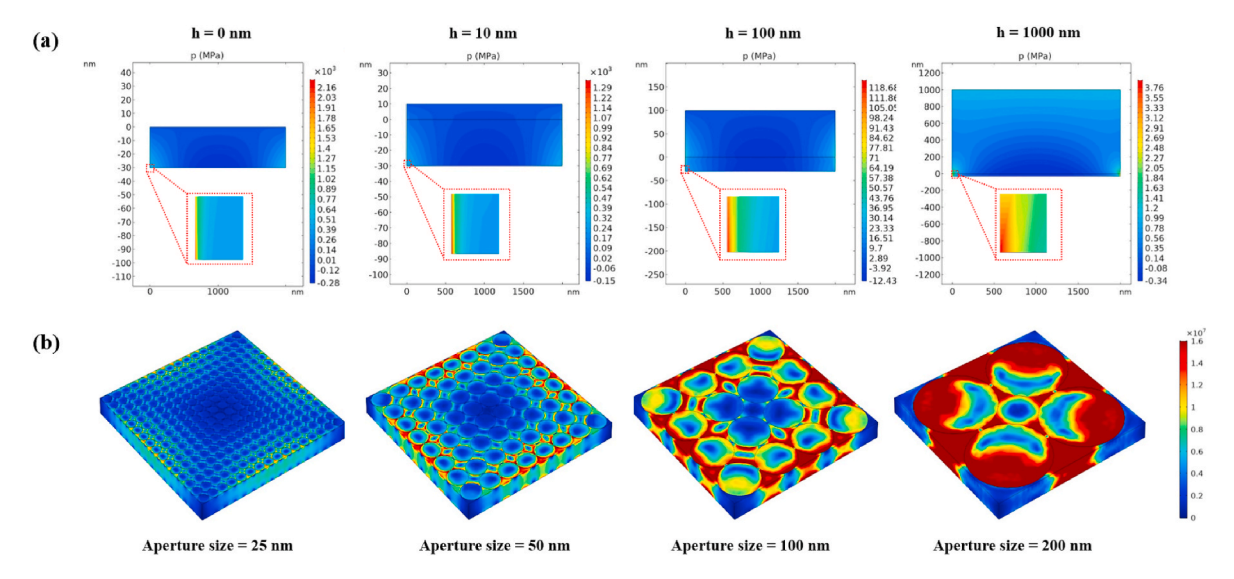


Fig. 2. Numerical simulation of the MCE thickness and aperture size effect on the stress distribution. (a) The cross-sectional tensile stress distribution on the GO laminates with the different thicknesses of the protective layer (h = 0, 10 nm, 100 nm, and 1000 nm respectively). (b) The tensile stress loaded on the GO laminates with different aperture sizes of the protective layer (25 nm, 50 nm, 100 nm, and 200 nm respectively).

MPa. In this case, the MCE thickness should be >100 nm for long-time stability. On the other hand, the water flux of a commercialized MCE membrane with 100-µm thickness was still as high as 72 L/m^2 h according to the simulation results in Fig. S1. The bottleneck for a highwater permeability was still the GO laminates instead of the MCE membrane.

Besides the thickness of the protective layer, the aperture size is another variable to affect the hydrodynamic stress which may lead to the failure of GO laminates. Similar to the thickness issue, a small aperture could reduce the hydrodynamic force and also downsize the water flow. Fig. 2 (b) shows the hydrodynamic stress distribution on the 30-nm thick GO laminates which have fixed boundaries on the side with different aperture sizes. In order to visually compare the effect of aperture size on the tensile stress, the scale label for all the simulation results shown in Fig. 2(b) was set to be the same. The largest stress occurs at the edge of the 200 nm-pore MCE layer was found to 268 MPa. In this situation, the GO laminates will be cracked since the strength of the 30-nm GO laminate is < 180 MPa, resulting in a failure of the RO desalination. When a 25 nm-pore MCE layer was used, the largest stress loaded on the GO laminates was calculated to 16 MPa, almost one order of magnitude lower than that in the case of the 200 nm-pore MCE layer. Obviously, the hydrodynamic stress loaded on the GO laminates was very sensitive to the aperture size of the MCE layer. Based on the tensile test of ultrathin GO laminate, the strength was dependent on the GO lateral size. For <500 nm GO nanosheets, the resultant laminates showed a tensile strength of ~120 MPa (Fig. S3), and thus the aperture size of the protective layer should be < 130 nm for robust desalination performance (rupture of the membrane could lead to very poor ion rejection). In addition, the effect of the MCE aperture size on water flux was also examined. The MCE aperture size was on the order of 10 nm, which was large enough to fit the Hagen Poiseuille (HP) Equation [34]. Hence, the water flux for different apertures can be calculated through HP Equation. The size of the aperture was positively related to the water flow. The water flux for a 25-nm aperture was 86 L/m² h, much larger than that for the GO laminates. The calculation results for the effect of aperture size on the tensile stress and water flux are shown in Fig. S1. Therefore, the selection of the aperture size for the protective layer should be based on the loaded stress on GO, and ensure it is less than the maximum strength of GO laminates while the water flow stays as large as possible. Since the tensile strength of GO laminates was on the order of 100 MPa according to the tensile tests (shown in Fig. S3) and the data from reference [35], a 25 nm-pore MCE was used for this study.

As mentioned before, the energy consumed by RO membranes for the membrane filtration process accounts for over 71% of the overall energy in the water desalination [6]. In this research, the GO-based gradient membrane was designed to reduce the energy consumption in the RO desalination process while the high water-permeability and high ion-rejection were maintained. A single film of GO laminates demonstrated channels around 0.7-1.1 nm caused by moistures, but it could swell and expand the interlayer spacing to 1.35 nm[29,36,37]. Cross-linking GO with desired constant interlayer spacing is essential in the RO desalination for stable performance. Compared with other cross-linkers, such as cations [29], fullerene (C_{60}) [31], 1, 4-phenylene diisocyanate (PDI) [30], and ethylenediamine (EDA), p-phenylenediamine (PPD) shows proper interlayer spacing as well as high robustness in water surroundings [38]. Unlike linear diamine monomer, PPD exhibits higher stiffness because of the presence of a benzene ring which has a fixed molecular length. In the GO-PDD membrane, GO membrane was functionalized with negatively charged functional groups such as -COOH and -OH. Thus, anions (Cl⁻) can be excluded at the entrance by electrostatic exclusion and steric effects [39]. Cations (Na⁺) can be excluded by the steric effects because Na⁺ has a larger hydrate diameter (7.2 Å) [40]. The detailed route of synthesizing GO-PPD composite is shown in Fig. 3 (a) and Method Section.

For energy saving, one feasible strategy is to reduce the watertransport pathway in the RO membrane since the energy losses from friction can be reduced. The water-transport pathway is determined by the thickness of the membrane as well as the lateral size of each GO nanosheet. To investigate the effect of GO nanosheet lateral size on the performance of water desalination, GO dispersion was treated by tip sonication before further crosslinking. The average lateral sizes of GO nanosheets with different treatment time (0 min, 3 min, 10 m min, 20 min) were measured to 1430 nm, 1009 nm, 473 nm, and 276 nm, respectively. DLS and the AFM characterizations are shown in Fig. 3 (b). The zeta potential of resultant solutions was also measured to understand the stability and nanomaterial distributions. At pH \approx 10, the zeta potential for the solution of pure GO and GO-PDD solution were -45.2 mV and -15.7 mV, respectively. The XRD patterns and ATR-FTIR spectrums were provided in Figs. S4 and S5 to address the interlayer spacing of GO laminates and the chemical reaction between GO and PPD monomer, respectively. The average interlayer spacing of pure GO, uncrosslinked GO-PPD, and crosslinked GO-PPD was found to 0.77 nm, 1.0 nm, and 1.1 nm, respectively. The expansion of interlayer spacing was caused by the collective effect of the molecular length of PPD monomer Y. Liu et al. Composites Part B 202 (2020) 108426

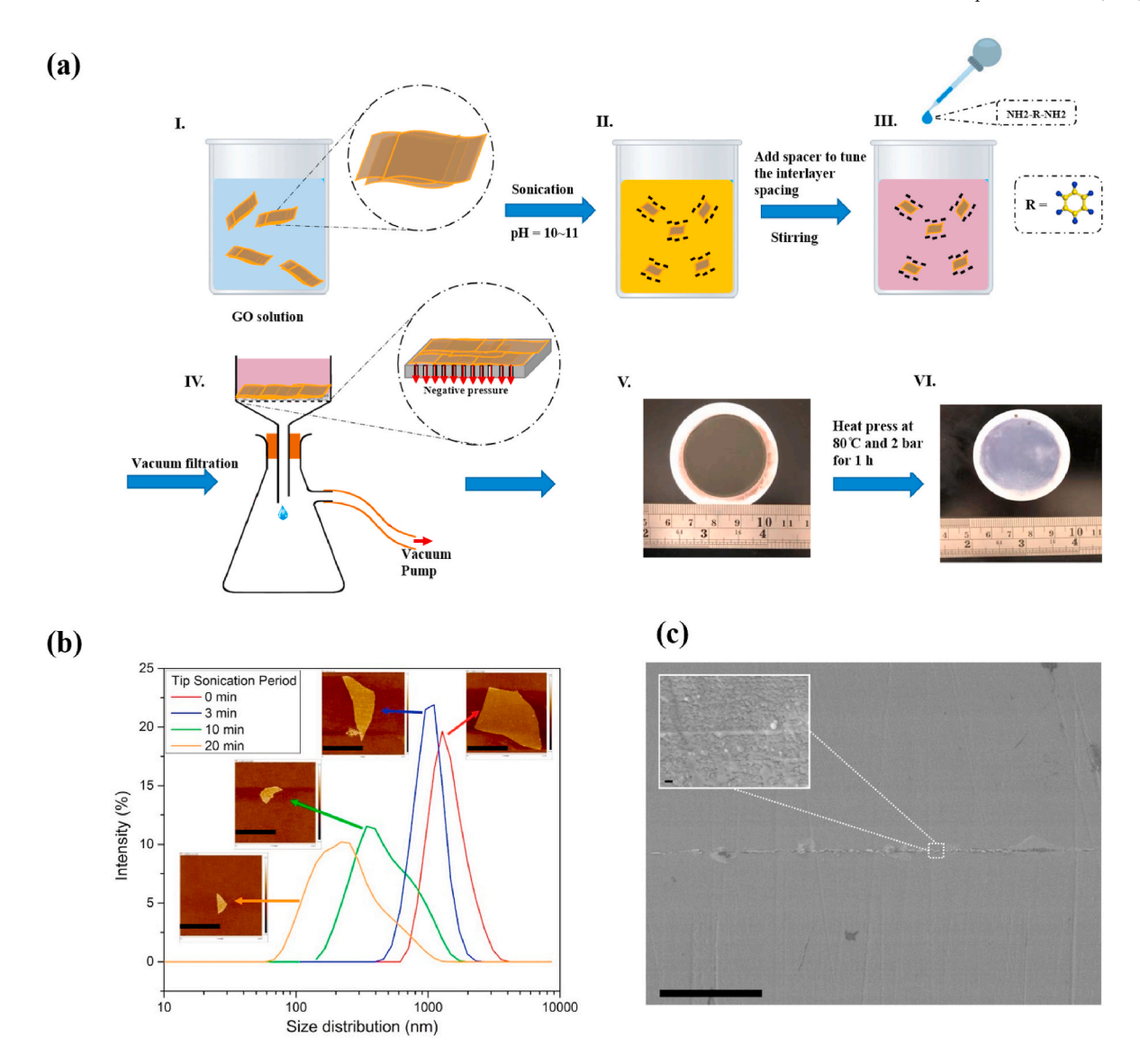


Fig. 3. Schematic illustration of gradient MCE/GO/MCE gradient nanocomposite membrane fabrication and corresponding experimental characterizations. (a) The fabrication procedure of the gradient nanocomposite membrane. (b) DLS results and AFM images of GO nanosheets with different tip sonication time (0 min, 3 min, 10 min, and 20 min), resulting in a GO lateral size with 1430 nm, 1009 nm, 473 nm, and 276 nm, respectively. The scale bars for the insert AFM image are 1 μm. (c) A SEM image of nanocomposite membrane cross-section. The scale bar in the large image is 100 μm while the scale bar in the insert magnification image is 100 nm.

as well as the C–N bond on both sides between PPD monomers and GO nanosheets. The gradient structure was achieved by covering a filtrated untreated GO-PPD membrane (Fig. 3 (a) Step V.) with another MCE membrane as the protective layer followed by hot-pressing at a constant pressure and temperature to crosslink the gradient membrane. The hydroxyl group in the cellulose acetate can react with the epoxy group on GO to create a strong chemical bond between GO laminates and the MCE membrane [41]. Fig. 3 (c) shows the cross-sectional SEM image of the gradient structure after crosslinking. The inset image indicates the sub-100 nm GO laminates encapsulated in the middle of the MCE membrane. The surface morphology and corresponding surface roughness are shown in Fig. S6.

To examine the effect of GO-PPD laminates thickness and the lateral size of GO nanosheets on water permeability and ion rejection rate, the desalination tests were carried out using the nanocomposite membrane made from GO laminates with different thicknesses (30 nm, 60 nm, 90 nm, and 150 nm on average), and different GO nanosheet sizes (1430 nm, 1009 nm, 473 nm, and 276 nm). The 2000 ppm (0.034 M) NaCl water was used as feed water and the applied pressure was 2.68 bar,

which means 1 bar left after overcoming osmotic pressure. The desalination results are shown in Fig. 4 (a) and (b) while the inserted image shows the test setup. The whole device was operating under magnetic stirring to avoid the influence of the concentration polarization effect on the feed side. The thinner GO-PPD laminates exhibited higher water permeability because of the shorter water-transport pathway, which reduced the friction during the water molecule. The ion rejection rate slightly went up for the increased thickness of the GO laminate because thicker GO-PPD laminates induced a larger steric effect to reject the salt ion. On the other hand, the enhancement of water permeability using smaller GO nanosheets can be also ascribed to the reduction of the water-transport pathway. As shown in the insert image of Fig. 4 (a), the smaller lateral size of GO nanosheets provides a shorter and less tortuous water-transport pathway, indicating smaller friction losses during the molecule transportation. The effect of GO lateral size on the ion rejection was negligible. Consequently, the gradient nanocomposite membrane made from the 30 nm-thick GO-PPD laminates with 476 nm GO nanosheets demonstrated a water permeability of 21.34 L h⁻¹ m⁻² bar⁻¹ and an ion rejection rate of 96.08%.

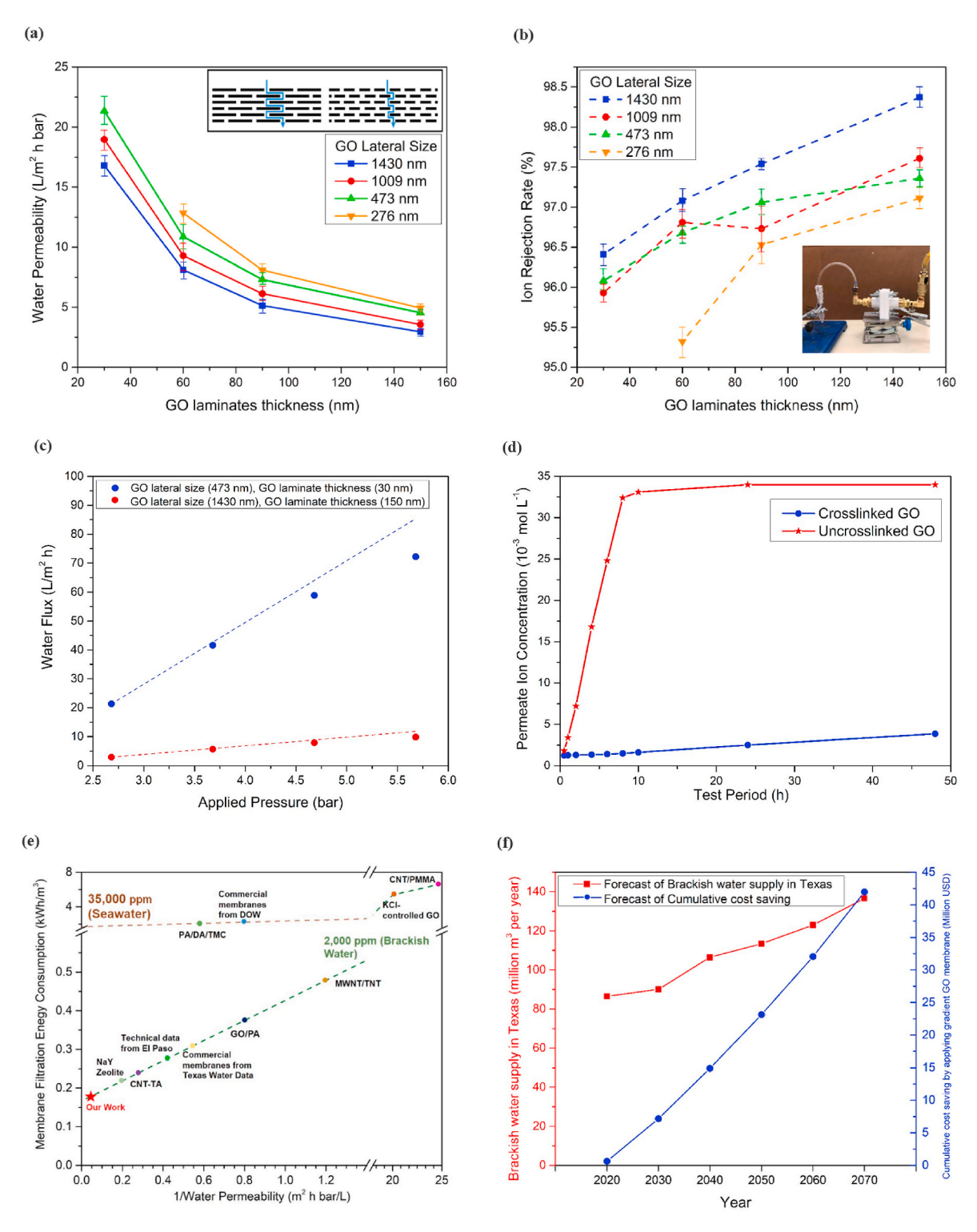


Fig. 4. Desalination performance of gradient nanocomposite membrane. (a) The water permeance for the gradient nanocomposites membrane with different thicknesses of GO laminates and different lateral sizes of GO sheets. The inserted image shows the water-transport pathway through the GO laminates. (b) The ion rejection rate for the gradient nanocomposites membrane with different thickness of GO membrane and different lateral size of GO sheets. The inserted image shows the test setup. (c) The water flux at different applied pressure. The dashed line indicates the linear trend without the concentration polarization issue. (d) The ion concentration on the permeation side through gradient membrane at different periods (the red and blue lines represent the uncrosslinked GO laminates and crosslinked GO laminates, respectively). (e) Comparison of the energy consumption between this work and the state-of-the-art RO desalination membranes including commercial membranes [6] and PA/DA/TMC [44] for 35,000 ppm seawater and commercial membranes [45], CNT-TA membranes [46], NaY Zeolite membranes [47], MWNT/TNT membranes [48], KCl-controlled GO membranes [29], CNT/PMMA membranes [49], GO/PA membranes [50], and technical data from El Paso Water Utilities for 2000 ppm brackish water. (f) The forecast of future brackish water supply and corresponding cumulative cost saving by applying the gradient nanocomposite membranes. (For interpretation of the references to color in this figure legend, the reader is referred to the Web version of this article.)

Y. Liu et al. Composites Part B 202 (2020) 108426

The effect of applied pressure on the water flux is critical for the water desalination process. When pure water passes through the RO membrane, the water flux increases linearly with the applied pressure. For the salinity filtration, the salt ions which are retained by the GO laminates can form a thin layer of concentration polarization or even a cake layer [42]. Both these effects could boost the resistance of the membrane to water flux and thus cause the pressure to drops across the membrane. As such a layer was getting thicker, the driven pressure for the filtration process was becoming smaller due to the increasing flow resistance. When the driven pressure became smaller than the local osmotic pressure, the water molecules cannot pass through the membrane. The experimental results are shown in Fig. 4(c) for two different lateral sizes of GO nanosheets. The dashed lines show the trends without the polarization issue. The smaller lateral size of GO nanosheets (473 nm) was usually related to a smaller polarization effect because a smaller water flux only took fewer salt ions to the surface of GO laminates. As a result, a larger applied pressure was needed for a stable water flux. Energy saving from previous studies was very marginal after the permeability is over 25 L h⁻¹ m⁻² bar⁻¹ where energy consumption was already intensive [43]. Since energy consumption is positively related to the applied pressure, it is vital to operate the desalination process at the low applied pressure range where the polarization issue does not significantly reduce the water permeability.

The ion rejection rate stability and membrane lifetime are also important factors to evaluate the potential of commercialization. Stability relies on two aspects of the membrane, the stability of interlayer spacing, and the robustness of the membrane. A stable interlayer spacing and a robust membrane can provide a long-term ion sieving effect. Most reported GO-based membranes can be effectively used for ion sieving for 5-10 h [29]. Here, the stability of the gradient nanocomposite membrane was also tested. For comparison, the crosslinked GO laminates and uncrosslinked GO laminates were both integrated to a gradient structure with a protective and supporting layer. As shown in Fig. 4 (d), for the uncrosslinked GO, the ion concentration of the permeate side increased rapidly from the beginning to 8 h until the concentration was almost equal to the feed side. This issue was caused by the swelling effect of GO laminates in the water surroundings which enlarged the interlayer spacing of GO laminates to allow salt ions passing through. In contrast, the ion concentration of the permeate side for the crosslinked gradient GO membrane demonstrates a negligible increase, indicating excellent stability and lifetime. In the crosslinked GO laminates, covalent bonds between GO and PPD molecule were much stronger than the hydrogen bonds between pure uncrosslinked GO, and thus provided stable interlayer spacing for long-term stability.

The overall energy consumption for RO desalination is contributed by the RO filtration process and other processes (e.g. pretreatment of water, etc.), which are not related to the RO membrane. In this study, the energy consumption related to other processes were regarded as fixed in order to reveal the energy consumption of gradient nanocomposite membranes. The energy consumption contributed by sole RO filtration process disclosed the performance of the water desalination process, and was defined as the membrane filtration energy consumption (SEC_f), a part of the total specific energy consumption (SEC). The SEC for seawater desalination is 3.57 kWh/m³ and the SEC_f accounts for 71% of it as shown in Fig. S8 [6]. On the other hand, although a lot of research has been made to investigate the water permeability of various membranes, it was very difficult to compare their performance due to different test conditions, such as feed salinity, salt composition, or applied pressure. Therefore, it is important to generate a unified criterion to quantify the energy consumption for different RO membranes. Here, a unified model was established to quantify the energy consumption for a given RO membrane with given water permeability, feed salinity, feed flow, and feed pressure.

According to the hydrodynamic theory, the membrane filtration energy consumption (SEC $_{\rm f}$) can be derived and the details were provided in the supplementary:

$$SEC_{f} = \frac{1}{\eta} \cdot \frac{P_{in} - \xi(1 - R)(P_{in} - P_{lost})}{R}$$
 (5)

where ξ was the efficiency of the pressure recovery process, R was the recovery rate, and P_{lost} was a numerical function of P_{in} [7].

For a given feed salinity, the feed pressure P_{in} can be also derived from the water permeability as detailed in the Supplementary Materials. Therefore, assuming the energy consumed by water intake, pretreatment, product water delivery, pump & ERD inefficiency, the energy consumed by membrane filtration for RO membranes can be estimated based on the water permeability, the applied pressure, and the salinity concentration [51]. Briefly, the energy consumption was a function of the applied pressure, pressure loss in the flow resistance, and water flux. For example, the water permeability of the gradient nanocomposite membrane was 21.34 L h⁻¹ m⁻² bar⁻¹ and the feed salinity was 2000 ppm NaCl solution. According to supplementary Eqs. (S4)-(S11), the SEC for the gradient nanocomposite membrane was calculated to 0.169 kWh/m [3]. Following the same procedure, the numerical relationship between the water permeability and the corresponding SEC for the given feed salinity was plotted as shown in Fig. S9. The blue line and the green line indicated the SEC for 35,000 ppm seawater and 2000 ppm brackish water respectively. Considering the constant energy consumption of the RO desalination process induced by water intake, pretreatment, product water delivery, and other facilities, the overall energy consumption is shown in Fig. S9.

In addition, Fig. 4(e) also shows the comparison of the membrane filtration energy consumption between this work and the state-of-the-art RO desalination membranes including commercial membranes [6] and PA/DA/TMC [44] for 35,000 ppm seawater and commercial membranes [45], CNT-TA membranes [46], NaY Zeolite membranes [47], MWNT/TNT membranes [48], KCl-controlled GO membranes [29], CNT/PMMA membranes [49], GO/PA membranes [50], and technical data from El Paso Water Utilities for 2000 ppm brackish water). Only the state-of-the-art RO membranes whose ion rejection rate larger than 90% for NaCl salinity were taken into account. The membrane filtration energy of the gradient nanocomposite membrane was 0.169 kWh/m³ which was 35.8% less than that of commercial membranes for 2000 ppm brackish water. As the forecast by Texas Water Development Board [52], the usage of brackish water desalination would be 90 million m³ in 2030 and 140 million m³ in 2070. Assuming the energy consumption accounts for 60% of the total cost [5], the cumulated cost saving from the gradient nanocomposite membranes until 2030 can reach 7.2 million for Texas. The forecast of brackish water supply and corresponding cumulative cost saving by applying gradient GO membranes is shown in Fig. 4 (f).

The scalability of the nanocomposite membranes was also examined because the scalability is a key factor to evaluate the commercial potential of a scientific and engineering design. In contrast, many membranes like aquaporin [20,53,54], and nanoporous graphene [35,55,56] achieved high water permeability desalination membranes but their scalability was very poor [57]. Fig. 5(a) shows the as-prepared scale-up gradient nanocomposite membrane with a 30-cm diameter. Instead of vacuum filtration, the pressure-driven filtration method was applied to the scale-up fabrication of gradient nanocomposite membrane. A scale-up membrane was readily demonstrated where GO laminates were 432 nm thick on average. The only issue with scale-up lies in the lower-bound of GO laminate thickness in the large-scale nanocomposite membranes in order to fabricate the uniform and non-defect GO membrane on a large scale. It was a little higher than that in the small-scale nanocomposite membranes. The water desalination performance was tested under the same condition as the small-size nanocomposite membranes. The water permeability was found to $0.81 \, \mathrm{Lh^{-1} \, m^{-2} \, bar^{-1}}$ while the ion rejection rate was still as high as 97.36%. Compared with the small-size gradient nanocomposite membrane, the scale-up membrane demonstrated a lower water permeability because of an increased lower bound of GO laminates thickness. On the other hand, as shown in

(a)



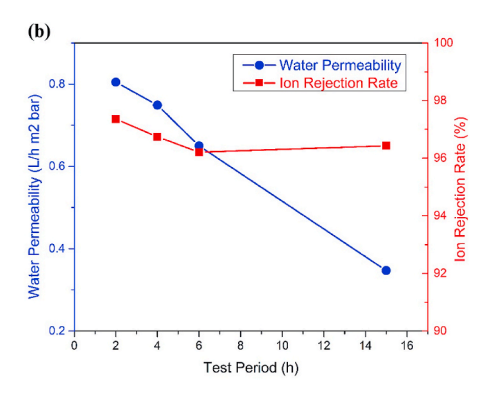


Fig. 5. Scale-up demonstration of gradient nanocomposite membrane. a, As-prepared scale-up gradient nanocomposite membrane. b, The ion concentration on the permeation side through gradient membrane and ion rejection rate at different periods for scale-up gradient GO membranes (the red and blue lines indicate the permeate ion concentration ion rejection rate respectively). (For interpretation of the references to color in this figure legend, the reader is referred to the Web version of this article.)

Fig. 5(b), the ion concentration of the permeate side for the scale-up gradient nanocomposite membrane confirmed excellent stability and lifetime. Further research is needed to tailor the thinner and uniform GO laminates at a large scale for larger water permeability and commercialization.

4. Conclusion

In summary, a gradient nanocomposite membrane has been demonstrated through simulation-guided design. The simulation results suggested that the protective layer should be > 100 nm thick with < 130 nm pores at a porosity of 72%. As-fabricated nanocomposites membranes exhibit water permeance as high as 21.34 L $\rm h^{-1}~m^{-2}~bar^{-1}$ and ion rejection rate >96.08%, indicating a 35.8% energy saving on membrane filtration for brackish water and the cumulative cost savings for Texas was estimated to 7.2 million in 2030 by applying the gradient nanocomposite membranes for brackish water RO desalination. The unique gradient structure supplies optimal protection for the ultrathin GO laminates, which not only contributes to the high water permeability and consequently low energy consumption but also the effective reduction for tensile stress to extend the membrane lifetime. These results afford a new direction to design and fabricate scalable RO membrane for energy-efficient water desalination.

CRediT authorship contribution statement

Yuchen Liu: Investigation, Software, Validation, Writing - original draft. Zimeng Zhang: Investigation. Wei Li: Investigation. Ruochen Liu: Investigation. Jingjing Qiu: Writing - review & editing. Shiren Wang: Conceptualization, Funding acquisition, Methodology, Supervision, Writing - review & editing.

Declaration of competing interest

There is no conflict of interest regarding this research.

Acknowledgment

The authors are grateful to the funding support from Water Research Grant by The State of Texas. This research is also partially supported by the National Science Foundation (CMMI #1634858 and CMMI#1934120).

Appendix A. Supplementary data

Supplementary data to this article can be found online at https://doi.org/10.1016/j.compositesb.2020.108426.

References

- Teow YH, Mohammad AW. New generation nanomaterials for water desalination: a review. Desalination 2019;451:2–17.
- [2] Elimelech M, Phillip WA. The future of seawater desalination: energy, technology, and the environment. science 2011;333(6043):712–7.
- [3] Liu Q, Xu G-R. Graphene oxide (GO) as functional material in tailoring polyamide thin film composite (PA-TFC) reverse osmosis (RO) membranes. Desalination 2016; 394:162–75.
- [4] García-Pacheco R, Landaburu-Aguirre J, Terrero-Rodríguez P, Campos E, Molina-Serrano F, Rabadán J, Zarzo D, García-Calvo E. Validation of recycled membranes for treating brackish water at pilot scale. Desalination 2018;433:199–208.
- [5] Zarzo D, Prats D. Desalination and energy consumption. What can we expect in the near future? Desalination 2018;427:1–9.
- [6] Voutchkov N. Energy use for membrane seawater desalination–current status and trends. Desalination 2018;431:2–14.
- [7] Cohen-Tanugi D, McGovern RK, Dave SH, Lienhard JH, Grossman JC. Quantifying the potential of ultra-permeable membranes for water desalination. Energy Environ Sci 2014;7:1134–41.
- [8] Karabelas A, Koutsou C, Kostoglou M, Sioutopoulos D. Analysis of specific energy consumption in reverse osmosis desalination processes. Desalination 2018;431: 15–21
- [9] Thomas JA, McGaughey AJ. Reassessing fast water transport through carbon nanotubes. Nano Lett 2008;8(9):2788–93.
- [10] Su J, Guo H. Effect of nanochannel dimension on the transport of water molecules. J Phys Chem B 2012;116(20):5925–32.
- [11] Werber JR, Osuji CO, Elimelech M. Materials for next-generation desalination and water purification membranes. Nature Reviews Materials 2016;1(5):16018.
- [12] Shi Q, Zhang K, Lu RF, Jiang JW. Water desalination and biofuel dehydration through a thin membrane of polymer of intrinsic microporosity: atomistic simulation study. J Membr Sci 2018;545:49–56.
- [13] Akhavan M, Schofield J, Jalili S. Water transport and desalination through double-layer graphyne membranes. Phys Chem Chem Phys 2018;20(19):13607–15.
- [14] Wei GL, Quan X, Chen S, Yu HT. Superpermeable atomic -thin graphene membranes with high selectivity. ACS Nano 2017;11(2):1920–6.
- [15] Humplik T, Lee J, O'hern S, Fellman B, Baig M, Hassan S, Atieh M, Rahman F, Laoui T, Karnik R. Nanostructured materials for water desalination. Nanotechnology 2011;22(29):292001.
- [16] Zhao F-Y, Ji Y-L, Weng X-D, Mi Y-F, Ye C-C, An Q-F, Gao C-J. High-flux positively charged nanocomposite nanofiltration membranes filled with poly (dopamine) modified multiwall carbon nanotubes. ACS Appl Mater Interfaces 2016;8(10): 6693–700.
- [17] Zhang C, Wei K, Zhang W, Bai Y, Sun Y, Gu J. Graphene oxide quantum dots incorporated into a thin film nanocomposite membrane with high flux and antifouling properties for low-pressure nanofiltration. ACS Appl Mater Interfaces 2017;9(12):11082-94.
- [18] Song X, Zambare RS, Qi S, Sowrirajalu BN, James Selvaraj AP, Tang CY, Gao C. Charge-gated ion transport through polyelectrolyte intercalated amine reduced graphene oxide membranes. ACS Appl Mater Interfaces 2017;9(47):41482–95.
- [19] Chen B, Jiang H, Liu X, Hu X. Molecular insight into water desalination across multilayer graphene oxide membranes. ACS Appl Mater Interfaces 2017;9(27): 22826–36.
- [20] Tang C, Wang Z, Petrinić I, Fane AG, Hélix-Nielsen C. Biomimetic aquaporin membranes coming of age. Desalination 2015;368:89–105.
- [21] Liu Y, Zhang Z, Wang S. Carbon nanopore-tailored reverse osmotic water desalination. ACS ES&T Water 2020. https://doi.org/10.1021/ acsestwater.0c00015
- [22] Russo CJ, Golovchenko JA. Atom-by-atom nucleation and growth of graphene nanopores. P Natl Acad Sci USA 2012;109(16):5953–7.
- [23] Surwade SP, Smirnov SN, Vlassiouk IV, Unocic RR, Veith GM, Dai S, Mahurin SM. Water desalination using nanoporous single-layer graphene. Nat Nanotechnol 2015;10(5):459-64
- [24] Yang Y, Yang X, Liang L, Gao Y, Cheng H, Li X, Zou M, Ma R, Yuan Q, Duan X. Large-area graphene-nanomesh/carbon-nanotube hybrid membranes for ionic and molecular nanofiltration. Science 2019;364(6445):1057–62.

- [25] Abraham J, Vasu KS, Williams CD, Gopinadhan K, Su Y, Cherian CT, Dix J, Prestat E, Haigh SJ, Grigorieva IV. Tunable sieving of ions using graphene oxide membranes. Nat Nanotechnol 2017.
- [26] Joshi R, Carbone P, Wang F-C, Kravets VG, Su Y, Grigorieva IV, Wu H, Geim AK, Nair RR. Precise and ultrafast molecular sieving through graphene oxide membranes. science 2014;343(6172):752-4.
- [27] Wang W, Eftekhari E, Zhu G, Zhang X, Yan Z, Li Q. Graphene oxide membranes with tunable permeability due to embedded carbon dots. Chem Commun 2014;50 (86):13089–92.
- [28] Gao SJ, Qin H, Liu P, Jin J. SWCNT-intercalated GO ultrathin films for ultrafast separation of molecules. J Mater Chem 2015;3(12):6649–54.
- [29] Chen L, Shi G, Shen J, Peng B, Zhang B, Wang Y, Bian F, Wang J, Li D, Qian Z. Ion sieving in graphene oxide membranes via cationic control of interlayer spacing. Nature 2017;550(7676):380.
- [30] Feng B, Xu K, Huang A. Covalent synthesis of three-dimensional graphene oxide framework (GOF) membrane for seawater desalination. Desalination 2016;394: 122.
- [31] Liu Y, Phillips B, Li W, Zhang Z, Fang L, Qiu J, Wang S. Fullerene-tailored graphene oxide interlayer spacing for energy-efficient water desalination. ACS Applied Nano Materials 2018;1(11):6168–75.
- [32] Joshi RK, Carbone P, Wang FC, Kravets VG, Su Y, Grigorieva IV, Wu HA, Geim AK, Nair RR. Precise and ultrafast molecular sieving through graphene oxide membranes. Science 2014;343(6172):752–4.
- [33] Yang Q, Su Y, Chi C, Cherian CT, Huang K, Kravets VG, Wang FC, Zhang JC, Pratt A, Grigorenko AN, Guinea F, Geim AK, Nair RR. Ultrathin graphene-based membrane with precise molecular sieving and ultrafast solvent permeation. Nat Mater 2017;16(12):1198.
- [34] Berkooz G, Holmes P, Lumley JL. The proper orthogonal decomposition in the analysis of turbulent flows. Annu Rev Fluid Mech 1993;25(1):539–75.
- [35] Cohen-Tanugi D, Grossman JC. Mechanical strength of nanoporous graphene as a desalination membrane. Nano Lett 2014;14(11):6171–8.
- [36] Nair R, Wu H, Jayaram P, Grigorieva I, Geim A. Unimpeded permeation of water through helium-leak-tight graphene-based membranes. Science 2012;335(6067):
- [37] Sun P, Wang K, Zhu H. Recent developments in graphene-based membranes: structure, mass-transport mechanism and potential applications. Adv Mater 2016; 28(12):2287–310.
- [38] Hung W-S, Tsou C-H, De Guzman M, An Q-F, Liu Y-L, Zhang Y-M, Hu C-C, Lee K-R, Lai J-Y. Cross-linking with diamine monomers to prepare composite graphene oxide-framework membranes with varying d-spacing. Chem Mater 2014;26(9): 2983–90.
- [39] Konatham D, Yu J, Ho TA, Striolo A. Simulation insights for graphene-based water desalination membranes. Langmuir 2013;29(38):11884–97.
- [40] Conway BE. Ionic hydration in chemistry and biophysics, vol. 12. Elsevier Science Ltd: 1981.
- [41] Kafy A, Sadasivuni KK, Akther A, Min S-K, Kim J. Cellulose/graphene nanocomposite as multifunctional electronic and solvent sensor material. Mater Lett 2015;159:20–3.

- [42] Zhang M, Song L. Pressure-dependent permeate flux in ultra-and microfiltration. J Environ Eng 2000;126(7):667–74.
- [43] Werber JR, Deshmukh A, Elimelech M. The critical need for increased selectivity, not increased water permeability, for desalination membranes. Environ Sci Technol Lett 2016;3(4):112–20.
- [44] Said M, Ebrahim S, Gad A, Kandil S. Toward energy efficient reverse osmosis polyamide thin-film composite membrane based on diaminotoluene. Desalination and Water Treatment 2017;71:261–70.
- [45] Connecting Texas water data workshops. Texas Water Development Board; 2018.
- [46] Baek Y, Kim HJ, Kim S-H, Lee J-C, Yoon J. Evaluation of carbon nanotubepolyamide thin-film nanocomposite reverse osmosis membrane: surface properties, performance characteristics and fouling behavior. J Ind Eng Chem 2017;56: 327, 34
- [47] Dong H, Zhao L, Zhang L, Chen H, Gao C, Ho WW. High-flux reverse osmosis membranes incorporated with NaY zeolite nanoparticles for brackish water desalination. J Membr Sci 2015;476:373–83.
- [48] Azelee IW, Goh P, Lau W, Ismail A, Rezaei-DashtArzhandi M, Wong K, Subramaniam M. Enhanced desalination of polyamide thin film nanocomposite incorporated with acid treated multiwalled carbon nanotube-titania nanotube hybrid. Desalination 2017;409:163–70.
- [49] nan Shen J, chao Yu C, min Ruan H, jie Gao C, Van der Bruggen B. Preparation and characterization of thin-film nanocomposite membranes embedded with poly (methyl methacrylate) hydrophobic modified multiwalled carbon nanotubes by interfacial polymerization. J Membr Sci 2013;442:18–26.
- [50] Chae H-R, Lee J, Lee C-H, Kim I-C, Park P-K. Graphene oxide-embedded thin-film composite reverse osmosis membrane with high flux, anti-biofouling, and chlorine resistance. J Membr Sci 2015;483:128–35.
- [51] Cohen-Tanugi D, McGovern RK, Dave SH, Lienhard JH, Grossman JC. Quantifying the potential of ultra-permeable membranes for water desalination. Energy Environ Sci 2014;7(3):1134–41.
- [52] The future of desalination in Texas. Texas Water Development Board; 2018.
- [53] Li X, Chou S, Wang R, Shi L, Fang W, Chaitra G, Tang CY, Torres J, Hu X, Fane AG. Nature gives the best solution for desalination: aquaporin-based hollow fiber composite membrane with superior performance. J Membr Sci 2015;494:68–77.
- [54] Ding W, Cai J, Yu Z, Wang Q, Xu Z, Wang Z, Gao C. Fabrication of an aquaporinbased forward osmosis membrane through covalent bonding of a lipid bilayer to a microporous support. J Mater Chem 2015;3(40):20118–26.
- [55] Cohen-Tanugi D, Grossman JC. Nanoporous graphene as a reverse osmosis membrane: recent insights from theory and simulation. Desalination 2015;366: 59–70.
- [56] Surwade SP, Smirnov SN, Vlassiouk IV, Unocic RR, Veith GM, Dai S, Mahurin SM. Water desalination using nanoporous single-layer graphene. Nat Nanotechnol 2015;10(5):459
- [57] Yang Z, Ma X-H, Tang CY. Recent development of novel membranes for desalination. Desalination 2018:434:37–59.